JACS
JOURNAL OF THE AMERICAN CHEMICAL SOCIETY

Article

Impact of oxygen vacancy occupancy on charge carrier dynamics in BiVO photoanodes

Shababa Selim, Ernest Pastor, Miguel García-Tecedor, Madeleine R Morris, Laia Francas, Michael Sachs, Benjamin Moss, Sacha Corby, Camilo A. Mesa, Sixto Gimenez, Andreas Kafizas, Artem A. Bakulin, and James R. Durrant

J. Am. Chem. Soc., **Just Accepted Manuscript** • DOI: 10.1021/jacs.9b09056 • Publication Date (Web): 30 Oct 2019

Just Accepted

is published by the American Chemical Society. 1155 Sixteenth Street N.W., Washington, DC 20036

Impact of Oxygen Vacancy Occupancy on Charge Carrier Dynamics in $BiVO_4$ Photoanodes

Shababa Selim,[1] Ernest Pastor,[1]* Miguel García-Tecedor,[2] Madeleine R. Morris,[1] Laia Francàs,[1] Michael Sachs,[1] Benjamin Moss,[1] Sacha Corby,[1] Camilo A. Mesa,[1] Sixto Gimenez,[2] Andreas Kafizas,[1,3] Artem A. Bakulin,[1] James R. Durrant[1]*

Corresponding authors: j.durrant@imperial.ac.uk; e.pastor11@imperial.ac.uk

[1]Department of Chemistry, MSRH, White City Campus, Imperial College London, W12 0BZ
[2]Institute of Advanced Materials (INAM), Universitat Jaume I, 12006 Castelló, Spain
[3]The Grantham Institute, Imperial College London, South Kensington, London SW7 2AZ

Abstract

Oxygen vacancies are ubiquitous in metal oxides and critical to performance, yet the impact of these states upon charge carrier dynamics important for photoelectrochemical and photocatalytic applications, remains contentious and poorly understood. A key challenge is the unambiguous identification of spectroscopic fingerprints which can be used to track their function. Herein, we employ five complementary techniques to modulate the electronic occupancy of states associated with oxygen vacancies *in situ* in $BiVO_4$ photoanodes, allowing us to identify a spectral signature for the ionisation of these states. We obtain an activation energy of ~0.2 eV for this ionisation process, with thermally activated electron de-trapping from these states determining the kinetics of electron extraction, consistent with improved photoelectrochemical performance at higher temperatures. Bulk, un-ionised states however, function as deep hole traps, with such trapped holes being energetically unable to drive water oxidation. These observations help address recent controversies in the literature over oxygen vacancy function, providing new insights into their impact upon photoelectrochemical performance.

Introduction

Thermodynamically stable defect states are an ever-present problem in many energy conversion technologies. Structural defects can severely impact upon the performance of optoelectronic devices such as solar cells and photoelectrochemical (PEC) cells.[1,2] Thus, great effort has been devoted to understand defect chemistry in the materials employed in such devices. In metal oxide based PECs, one of the most prominent types of defects are due to

oxygen vacancies (V_o) created when an oxygen atom is removed from the lattice, leading to the transfer of two electrons to adjacent metallic sites.[3–8] These defects typically generate shallow sub-bandgap states responsible for n-type doping[9] and substantially impact upon materials and device performance, as has been widely discussed for hematite (α-Fe_2O_3),[2,10] tungsten oxide (WO_3)[11,12], strontium titanate ($SrTiO_3$)[13–15] and bismuth vanadate ($BiVO_4$).[3–5] However, whilst the importance of oxygen vacancies has become established, the specific impact of these states on PEC (and photocatalytic) performance remains controversial and poorly understood.

Metal oxide oxygen vacancies have been proposed to impact on PEC performance through several mechanisms. On the positive side, they have been reported to improve light absorption,[16] increase the concentration of bulk carriers,[5,9] thus aiding transport.[9] The intrinsic doping resulting from these states enables space-charge layer generation at the metal oxide/electrolyte junction[17] which can drive charge separation under operational conditions.[18–20] On the other hand, such defects can induce detrimental structural and phase changes,[21] and have been reported to act as recombination centres that reduce quantum yields.[2] Most importantly, surface oxygen vacancies are often proposed to have a direct role in catalytic processes like water oxidation, impacting upon photocurrent onset potentials[2,10] and enabling surface adsorption processes that accelerate reactivity.[22,23] To date, most of the studies have focused on measuring the impact of oxygen vacancies on the overall PEC performance, often correlated with computational analyses of the electronic properties of these states. Studies that directly probe the impact of these vacancies upon the charge carrier separation, recombination, trapping, transport and interfacial catalytic processes which underlie PEC function have been relatively limited, and are often contradictory to date, thereby limiting our understanding of the impact of these states on PEC performance. Such studies have in particular been complicated by a lack of consensus over the spectral signatures of these states, resulting in significant ambiguities in the interpretation of spectroscopic analyses of oxygen vacancy function.

In this work, we employ a suite of complementary *in situ* modulation measurements to elucidate unambiguously the energetics of oxygen-vacancy-associated states in the widely studied metal oxide, $BiVO_4$, and the impact of the electronic occupancy of these states upon

the charge carrier processes that determine PEC water oxidation activity. $BiVO_4$ is a promising ternary oxide which has yielded record water oxidation photocurrents in excess of 6 mA cm^{-2} at 1.23 V_{RHE}.[24] Its conduction band is mainly of vanadium 3d character,[25,26] with oxygen vacancy formation leading to the localisation of electrons on neighbouring vanadium sites,[8] reducing them from V^{5+} to V^{4+} (in-depth study of the electronic structure can be found in references 25 and 26). We refer to these localised electronic states as V_{OV}^{5+}/V_{OV}^{4+} oxygen vacancy states to distinguish them from conduction band (CB) states, which for simplicity we label: V_{CB}^{4+} (occupied CB state) and V_{CB}^{5+} (unoccupied CB states).

In the study herein, we focus on a strong optical feature observed in transient spectroscopic studies of $BiVO_4$ around its bandgap (λ = 470 nm, see Figure 2 below).[27–29] This feature appears spectroscopically analogous to a similar feature observed in α-Fe_2O_3 (λ = 580 nm), which we have previously suggested to originate from unoccupied oxygen vacancy states in α-Fe_2O_3.[30,31] There is however considerable dispute over the assignment of these features in both metal oxides, with other studies relating this spectral feature to photogenerated holes that undergo water oxidation,[27,32–35] or suggesting this feature results from structural changes resulting from thermal effects of pulsed laser excitation.[28,36] Such controversies are symptomatic of our limited understanding of the optical signals observed following optical excitation of these metal oxides. Herein, we address these ambiguities by directly modulating the population of V_{OV}^{5+}/V_{OV}^{4+} states in $BiVO_4$ using five complementary electrochemical, thermal and all-optical methods. Remarkable agreement between these techniques allow us to identify the spectroscopic fingerprint for these states, their energetics and their impact upon charge carrier dynamics. Our combined optical and electrochemical data demonstrates that these oxygen vacancies do not have a direct catalytic activity towards water oxidation. Rather, we find that occupied V_{OV}^{4+} states are the primary loss pathway for photogenerated valence band holes, whilst unoccupied V_{OV}^{5+} states function as shallow electron traps and control the extraction of conduction band electrons (the majority carriers) to the external circuit.

Results and Discussion

This study employs flat, dense $BiVO_4$ photoanodes fabricated by metal-organic decomposition with a monoclinic scheelite structure as determined by X-ray diffraction (XRD) (see Figure S1 for XRD and UV-Vis data). X-ray photoelectron spectroscopy (XPS), a surface sensitive

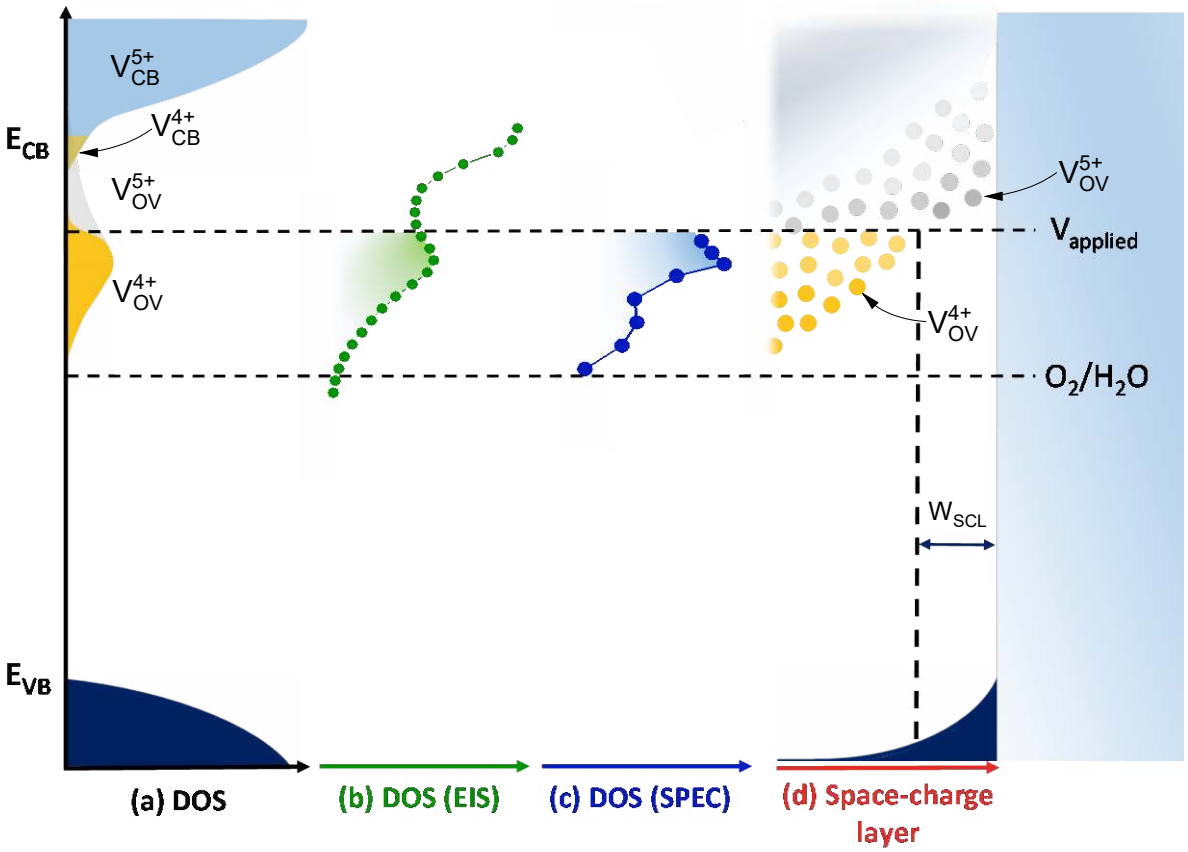

Figure 1| Schematic representation of sub-bandgap states associated with oxygen vacancies (amplified for illustration) in $BiVO_4$. a, Sub-bandgap states in relation to band edges. For illustration the yellow shaded regions represent occupied (reduced) states (V_{OV}^{4+}). **b**, Density of states (DOS), arising from the V_{OV}^{5+}/V_{OV}^{4+} redox couple associated with these defects, determined through capacitance data from impedance spectroscopy (green). **c**, DOS derived from spectroelectrochemistry measurements, tracking the optical absorbance at 470 nm as a function of applied bias (blue) (relative to the open-circuit potential of 0.6 V_{RHE}). **d**, Illustration showing the oxidation of V_{OV}^{4+} to V_{OV}^{5+} within the space-charge layer (W_{SCL}) at the semiconductor/electrolyte interface; yellow and grey circles represent occupied and unoccupied oxygen vacancy states, respectively.

technique, reveals that ~3-4% of all surface vanadium centres are in the V^{4+} state, indicating a surface oxygen vacancy density tentatively on the order of 1-2% per V centre (see Figure S2 for details). Photoelectrochemical (PEC) measurements reported herein were conducted in a three-electrode cell, unless stated otherwise. Photoelectrochemical water oxidation performance of the photoanodes is presented in Figure S3b, and is typical of such photoanodes reported in the literature.[19,37]

Dark electrochemical impedance analysis of our $BiVO_4$ photoanodes reveals the presence of a capacitance peak at ~0.8 V_{RHE}, as illustrated in Figure 1b (green trace) and Figure S3a. This capacitance is positive of the electrode flat band potential (E_{fb} ~0.35 V_{RHE}, Figure S3c) and coincides with the onset of photocurrent generation in these photoanodes (Figure S3b), both indicative of it being associated with space-charge layer formation at the electrode surface. Given that n-type doping of $BiVO_4$ primarily results from oxygen vacancies, this space charge layer formation, and the associated capacitance can be assigned to the depletion of V_{OV}^{4+} states, resulting in the formation of unoccupied (ionised) V_{OV}^{5+} states. This assignment is consistent with DFT calculations indicating shallow donor levels induced by oxygen vacancies in $BiVO_4$.[9,38] Therefore, the observed capacitance is assigned, as previously,[39] to the V_{OV}^{5+}/V_{OV}^{4+} couple.

To probe further the oxidation/reduction of V_{OV}^{5+}/V_{OV}^{4+} states and their impact upon charge carrier dynamics, we performed a series of differential absorption spectroscopy measurements. We start by modifying the sample electrochemically. We observe that the electrochemical oxidation of the $BiVO_4$ photoanode in the dark results in a strong absorption peak at 470 nm (Figure 2a). This absorption feature grows in amplitude with increasing anodic potential (Figure S4a). Differentiation of the optical signal as a function of applied potential allows us to determine the associated density of states (Figure 1c, see SI for details). Strikingly, we observe that the population distribution obtained from these spectroelectrochemical measurements correlates closely with the distribution of the V_{OV}^{5+}/V_{OV}^{4+} states obtained through impedance spectroscopy. This redox process, observed optically to correlate with an increase in unoccupied electronic states (V_{OV}^{5+}) below the conduction band (Figure 1c) is unlikely to be observed for the case of an electron polaron (discussed further in ESI, section 12), although we note that electrons trapped at oxygen vacancies are likely to induce wider lattice deformations analogous to those associated with such polarons. Based on this, we conclude that the 470 nm signal tracks the oxidation of the vanadium ions adjacent to oxygen vacancy sites from V_{OV}^{4+} to V_{OV}^{5+} and therefore is a direct probe of the V_{OV}^{5+} concentration. Consistent with this assignment, the dependence of the magnitude of this feature upon applied bias is in reasonable agreement with the expected potential dependence of the space-charge layer width attributed to oxygen vacancy ionisation (see Figure S3d and below for further discussion of this assignment). In the literature, charge localisation in $BiVO_4$ has been

proposed to lead to the formation of lattice distortions or polarons centred on vanadium atoms with several studies trying to identify these states. While the experiments we report herein do not provide structural information, the sensitivity of the 470 nm optical signal to the concentration of the V_{OV}^{5+}/V_{OV}^{4+} linked to oxygen vacancies can provide a powerful tool to explore phenomena directly influenced by the presence of such defects as well as their impact on catalysis.

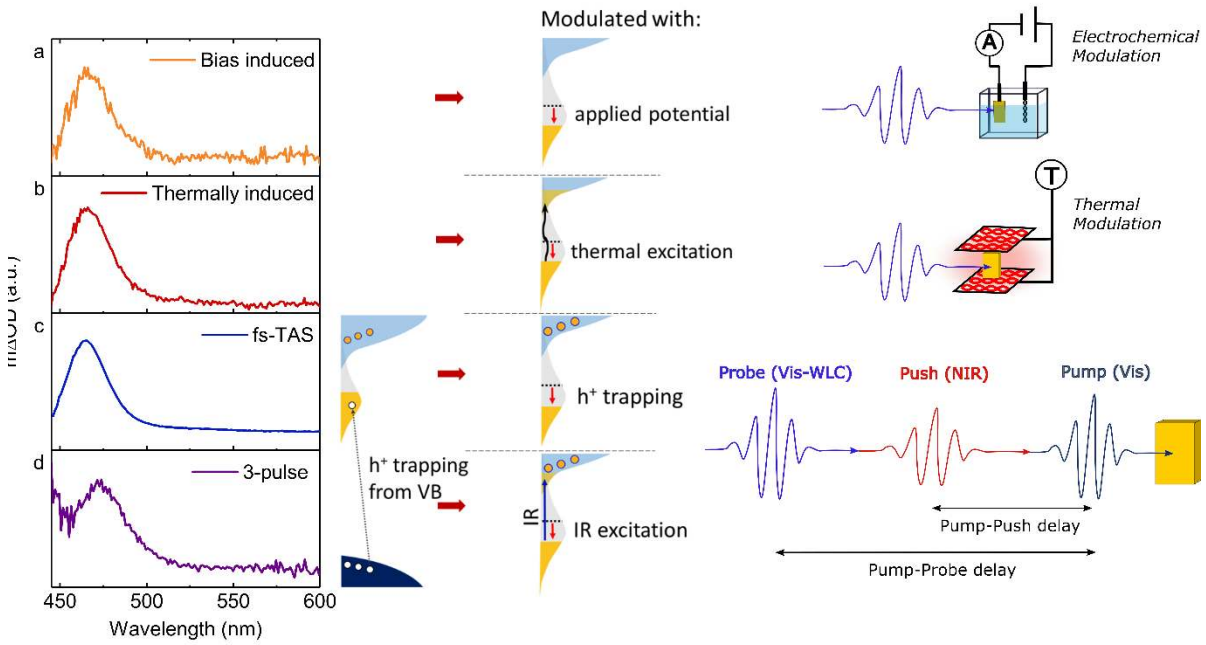

Figure 2| Difference spectra showing the optical absorption feature at 470 nm observed following the increase in the V_{OV}^{5+} concentration, modulated using four different techniques. a, Bias induced spectroelectrochemical difference spectrum, measured at 1.4 V_{RHE} relative to the spectrum at the open circuit potential (0.6 V_{RHE}) and assigned to the electrochemical oxidation of V_{OV}^{4+} to V_{OV}^{5+}. **b**, Thermally induced difference absorption spectrum measured at 301 K with respect to 295 K, assigned to thermal excitation of electrons from V_{OV}^{4+} to the conduction band. **c**, Transient absorption difference spectrum at 20 ps in electrolyte following excitation with λ_{ex}(*pump*) at 355 nm, assigned to oxidation of V_{OV}^{4+} states to V_{OV}^{5+} due to hole trapping into V_{OV}^{4+} states. **d**, 3-*pulse* UV *pump* – IR *push* – visible *probe* transient optical data, showing *push* ON minus *push* OFF spectrum measured at a 4 ps *push-probe* time delay, and assigned to electron excitation from V_{OV}^{4+} states into the conduction band by the IR (2060 nm, 0.6 eV) *push* pulse. All spectra were measured in 0.1 M phosphate buffer apart from **d**, which was measured in air. Further difference spectra as function of applied potential, temperature and time delay are shown in ESI (Figure S4).

In addition to applied bias, an alternative route widely used to modulate the ionisation of shallow dopant species in semiconductors is thermal heating, monitored most typically as a thermally induced increase in electrical conductivity.[40–42] In Figure 2b and S4b, we monitor

the dependence of the $BiVO_4$ absorption spectrum as a function of temperature, under open-circuit conditions in electrolyte. Increasing the temperature from 295 K to 301 K resulted in the appearance of an absorption at 470 nm, indistinguishable in shape from that induced electrochemically under anodic bias (see Figure S4b for data as a function of temperature). This thermally induced feature is therefore assigned to the thermally induced excitation of electrons from V_{OV}^{4+} states into the $BiVO_4$ conduction band (forming the V_{OV}^{5+} associated with the 470 nm feature as assigned above). Our observation that a small incremental increase in temperature results in a large optical signal (greater response than application of bias where oxidation is limited to the W_{SCL}, see Figures S4 for comparison between electrochemical *vs*. thermal response) confirms that these V_{OV}^{4+} states are energetically close to the conduction band edge. This is consistent with the density of states (DOS) determined through impedance and spectroelectrochemistry measurements (Figure 1), and with previous DFT calculations.[9,38] Furthermore, the similarity in the density of V_{OV}^{4+} states oxidised thermally and electrochemically (Figure S6) is a strong indication of the bulk distribution of the oxygen vacancy defects.

We now turn to transient absorption (TA) changes resulting from pulsed laser excitation of a $BiVO_4$ photoanode under open-circuit conditions. As shown in Figure 2c, the same ~470 nm spectral feature is observed in the transient absorption spectrum at 20 ps following bandgap excitation of $BiVO_4$ (see Figure S4c for the time delay dependence of this feature). Based on the thermal and electrochemical data reported above, this transient feature indicates that a photoinduced increase in concentration of V_{OV}^{5+} states (*i.e.* due to oxidation of V_{OV}^{4+} states) takes place shortly after photoexcitation. We rationalise this in terms of ultra-fast hole trapping of some photoinduced valence band holes into bulk V_{OV}^{4+} states, as illustrated in Figure 2 and discussed further below. This deep trapping process could also be described as equivalent to a recombination process between valence band holes and electrons trapped in shallow oxygen vacancy defect sites. This trapping/recombination process is likely to be a key determinant of bulk hole diffusion lengths in $BiVO_4$ (typically measured as ~100 nm).[40]

The final technique we employed to modulate the occupancy of $BiVO_4$ oxygen vacancy defect states is an optical, UV *pump* - IR *push* – visible *probe* technique, [43–45] a method previously applied to organic semiconductors,[43] but not to metal oxide photoelectrodes. This approach is similar to *pump-probe*, but uses the third low energy (2060 nm, 0.6 eV) *push* pulse to

selectively excite trapped electrons from shallow defect/dopant states into the conduction band. Figure 2d shows an enhancement of the feature at 470 nm in the *push* on-off TA spectrum in air, consistent with electron excitation out of V_{OV}^{4+} states (see Figures S7 for details). The ability of a 0.6 eV IR light pulse to excite electrons out of these oxygen vacancy states into the conduction band further confirms the assignment of the 470 nm optical feature to V_{OV}^{5+} concentration and also confirms that they are energetically close to the conduction band edge, as shown in Figure 1.

The results above allow us to explicitly assign the 470 nm optical absorption observed in our range of *in situ* modulation studies to V_{OV}^{5+}/V_{OV}^{4+} states located energetically close to the $BiVO_4$ conduction band. This near-edge absorption peak is analogous to an absorption feature observed in α-Fe_2O_3 at 580 nm, which we have previously associated with oxygen vacancy induced shallow trap states. [30,31,46] Our spectroelectrochemical data allows us to rule out that this feature results exclusively from thermally induced structural changes in $BiVO_4$, as suggested elsewhere.[28,36] The magnitude of change in the absorption signal following modest thermal heating indicates that these states are not confined to the $BiVO_4$ surface, but results from bulk oxygen vacancies. Crucially, the energetic location of these states, close to the conduction band, and different from those previously observed under ultra-high vacuum conditions,[47] allows us to rule out that this optical signal is associated with states directly involved in water oxidation, as suggested in several studies. [27,29,32–34] In particular, the 470 nm transient absorption feature has previously been reported for $BiVO_4$, but assigned to surface trapped holes that participate in water oxidation catalysis.[27,29] Similar conclusions have also been reported for the analogous feature in α-Fe_2O_3.[32–34] However, our impedance, spectroelectrochemical, thermally induced and IR *push* data all indicate that this feature originates from states lying energetically close to the conduction band edge (within ~0.2 eV, discussed below). As such, holes trapped in these states associated with this optical feature (*i.e.* V_{OV}^{5+} species) will be energetically unable to drive water oxidation (more negative than the thermodynamic water oxidation potential of 1.23 V_{RHE}). This conclusion is also consistent with our recent studies of charge trapping in oxygen vacancy states in tungsten oxide and points toward a general behaviour amongst n-type metal oxides.[12] We note the actual spectroscopic origin of the 470 nm signal we observe is less clear. Previously we have associated an analogous feature in α-Fe_2O_3,[30,31] to the optical excitation from the valence

band to ionised oxygen vacancies. However in $BiVO_4$, the energetics and the derivative-like nature of the spectral response suggest that the feature may be due to phenomena such as electroabsorbance effects, as suggested elsewhere.[28] Whilst further work is necessary to understand the exact spectroscopic origin of this optical feature, our experimental observations strongly correlate this spectral fingerprint to changes in the concentration of V_{OV}^{4+}/V_{OV}^{5+} oxidation states thus providing a means to reveal important information about the function of these states.

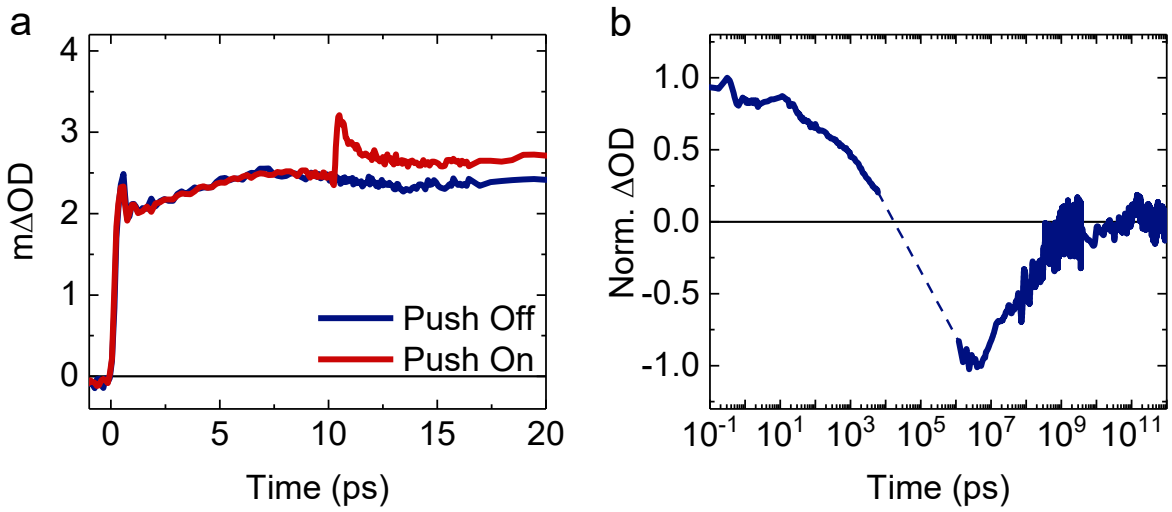

Figure 3| Kinetics associated with charge trapping into oxygen vacancy states. a, 3-pulse *pump-push-probe* measurement in air, showing the enhancement of the signal at 470 nm following *push* with 2060 nm pulse (3 mJ cm^{-2}) at a *pump-probe* time delay of 10.4 ps, following the initial *pump* excitation at 400 nm (200 µJ cm^{-2}). **b**, Normalised transient absorption kinetics spanning from fs-ns timescale probed at 470 nm, to the µs-s timescale probed at 460 nm (the dotted line is added to guide the eye). The film was excited with 355 nm (300 µJ cm^{-2}) under open circuit conditions in 0.1 M phosphate buffer.

We now consider the kinetics of charge trapping and de-trapping into and out of $BiVO_4$ oxygen vacancy states. Typical *pump* and *pump-push* induced transient absorption kinetics monitored at 470 nm are shown in Figure 3 (see Figures S7 – S9 for additional data, including measurements under anodic bias). The kinetics of the 470 nm absorption following bandgap excitation (Figure 3a, red trace and Figure S7a) are biphasic, exhibiting an instrument response limited (~200 fs) rise followed by a smaller ~10 ps increase in absorption. These rise kinetics are assigned to partial, deep hole trapping into bulk V_{OV}^{4+} states. This photo-induced absorption decays on the nanosecond timescale, and evolves on the microsecond timescale

into a transient bleach signal assigned to electron trapping into V_{OV}^{5+} states within the $BiVO_4$ space charge layer (Figure 3b and Figure S8). In agreement with this assignment, the magnitude of this long-lived bleach signal increases with anodic bias (Figure S9). The recovery of this bleach signal exhibits similar kinetics to those measured for charge extraction (Figure S9b), consistent with our assignment, and indicates that electron extraction is associated with electron release from V_{OV}^{4+} states. We note that these assignments and process timescales are in qualitative agreement with those reported previously for α-Fe_2O_3 and WO_3.[30,31,46,48] The additional 470 nm absorption induced by the IR *push* pulse decays on the nanosecond timescale (Figure S7a), indicating that the $BiVO_4$ CB electrons generated by this IR pulse tend to relax relatively slowly back into the ionised oxygen vacancy state from which they were excited. We also note that polaron formation is also likely to impact upon these charge carrier kinetics,[41,42,49] including the timescale of charge trapping into V_{ov} states, although a detailed discussion of such polaronic effects is beyond the scope of this study.

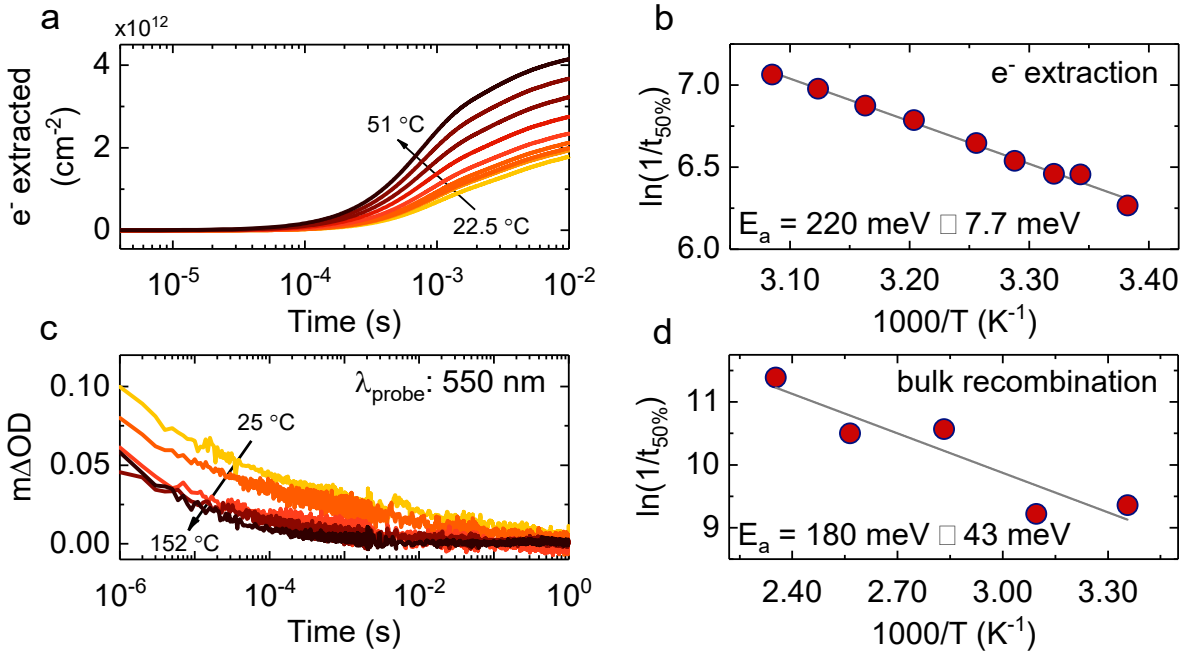

Figure 4| Temperature dependence of electron extraction and bimolecular recombination. a, Transient electron extraction from the $BiVO_4$ photoanode obtained with transient photocurrent measurements, measured at 0.6 V_{RHE} in 0.1 M phosphate buffer (pH 7) with λ_{ex}: 355 nm (300 μJ cm^{-2}). **b**, Activation energy for the electron extraction process. **c**, Transient absorption kinetics of holes in $BiVO_4$ in inert atmosphere (Ar) with λ_{pump}: 355 nm and λ_{probe}: 550 nm. **d**, Activation energy for the bulk recombination process.

Our results place $BiVO_4$ oxygen vacancy states energetically in close proximity to the CB edge, such that de-trapping of electrons from these states (i.e. ionisation of V_{OV}^{4+} to generate V_{CB}^{5+} states) is thermally activated, consistent with the thermally induced absorption changes reported above (Figure 2b). In order to investigate the importance of such thermally activated de-trapping on the PEC function of $BiVO_4$, we undertook further temperature dependence studies of charge extraction and recombination in $BiVO_4$. Figure 4a shows the temperature dependence of charge extraction (*i.e.* integrated photocurrent), measured at an applied bias near the photocurrent onset (0.6 V_{RHE}) where charge extraction is critically limited by electron de-trapping (Figure S9). It is apparent that with increasing temperature, the kinetics of charge extraction accelerate (Figure S10a) and the yield of extracted charge increases (Figure 4a). From the temperature dependence of the extraction half-time, we obtain an activation barrier of $E_{a,extraction}$ ~ 0.22 eV (Figure 4b). As these extraction kinetics also track the recovery of the transient bleach signal discussed above (Figure S9), this activation energy can be assigned to thermally induced release of electrons trapped as V_{OV}^{4+} to generate mobile charge carriers (most likely mobile small polarons). Figure 4c shows the decay kinetics of photoinduced bulk valence band holes in $BiVO_4$ measured in an inert atmosphere as a function of temperature, assigned to charge recombination. Again, the kinetics are observed to accelerate with increasing temperature (Figure S10b) with a very similar activation barrier ($E_{a,recombination}$ ~ 0.18 eV, Figure 4d). The similarity of these two activation energies suggests the kinetics of both processes are controlled by the thermal excitation of electrons from occupied oxygen vacancy states, enabling transport either to the external back contact (for electron extraction) or recombination with holes. Similar charge transport activation energies have previously been reported for $BiVO_4$ from thermal conductivity and current-voltage spectroscopy studies, although in these cases it was assigned to thermally activated small polaron hopping transport.[42,50] This ~0.2 eV activation energy we measure might explain why oxygen vacancies in $BiVO_4$ have a low doping efficiency, with the measured density of mobile electrons typically being several orders of magnitude lower than the measured density of oxygen vacancy sites. From a functional perspective, this ~0.2 eV activation energy can indicate that the doping efficiency of such photoelectrodes may be affected by the localisation of electrons in dopant (oxygen vacancy) states, thus limiting bulk conductivity,[51] which can be overcome at elevated temperatures. This is further reflected in the enhanced photoelectrochemical performance of $BiVO_4$ photoanodes operating at higher temperatures,

as shown in Figure S10c and reported previously.[52] Given that we observe accelerated electron extraction at elevated temperatures, we can attribute this higher performance of the $BiVO_4$ photoanodes to enhanced electron transport with increasing temperature.

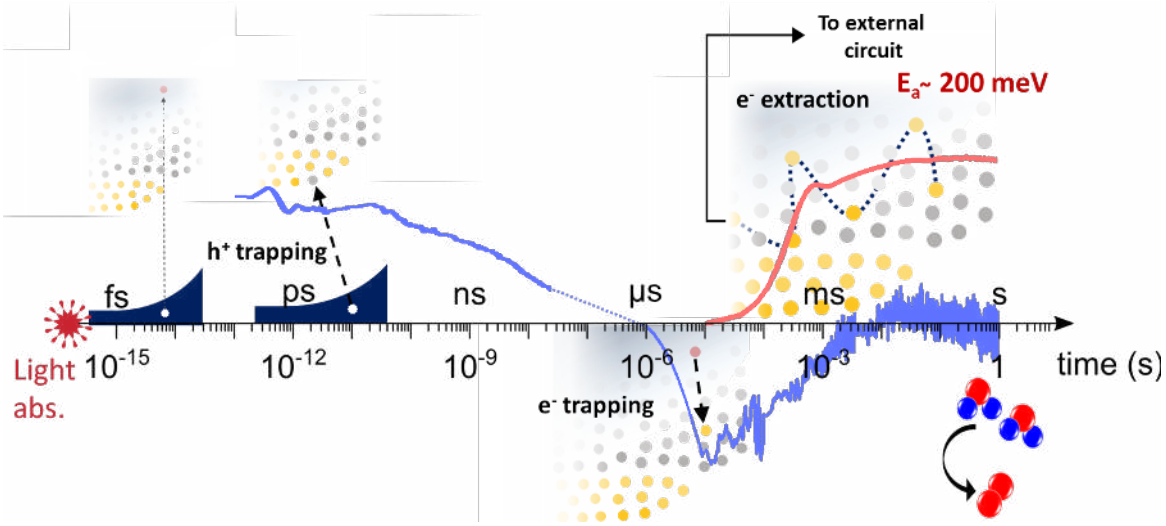

Scheme 1| Schematic illustration of the role of oxygen vacancies in charge carrier trapping and electron transport in $BiVO_4$ from the timescale of light absorption to water oxidation. Following charge generation, valence band holes trap into bulk V_{OV}^{4+} states leading to a positive TA signal (ps – ns). Within microseconds, electrons trap into V_{OV}^{5+} states within the space-charge layer causing the TA signal to bleach. On the millisecond timescale electrons are extracted though the electrical circuit causing the bleach to recover and the accumulated holes oxidise water. The charge extraction process takes place via thermal de-trapping from V_{OV}^{4+} with an activation barrier (E_a) of ~0.2 eV. For illustration, yellow states represent occupied V_{OV}^{4+} states, whereas grey states represent un-occupied V_{OV}^{5+} states.

Conclusions

Scheme 1 summarises some of the key functional processes underlying water oxidation in $BiVO_4$ photoanodes, and the role oxygen vacancies play. In addition to their role in space-charge layer formation and n-type doping of bulk $BiVO_4$ to reduce resistance losses during bulk charge transport, oxygen vacancy states participate in the trapping of photogenerated electrons and holes. In the bulk, hole trapping is a significant loss pathway, as this deep trapping is strongly exothermic, with the resultant oxidised oxygen vacancy states being energetically unable to drive water oxidation. On the other hand, electron trapping is reversible, with a de-trapping activation energy of ~0.2 eV. Such electron trapping occurs particularly in the space-charge layer, where most oxygen vacancies are ionised (unoccupied) in the dark, resulting in a thermally activated electron extraction into the external circuit.

Thermally activated electron extraction is consistent with enhanced PEC water splitting performance at higher temperatures, important for technological application of such photoanodes under one sun or concentrated sunlight. Given the prevalence of oxygen vacancy formation in metal oxides and their impact on the electronic structure,[11,30,31] the optimisation of oxygen vacancy ionisation may be used as a tool to increase the performance of metal oxide-based water splitting devices.

Acknowledgements

We thank Prof Ian D. Sharp for helpful discussions. J.R.D. acknowledges financial support from the European Research Council (project Intersolar 291482). S.S. and B.M acknowledges EPSRC for DTP studentships. A.K. thanks Imperial College for a Junior Research Fellowship, the EPSRC for a Capital Award Emphasising Support for Early Career Researchers and the Royal Society for an Equipment Grant (RSG\R1\180434). A.A.B is a Royal Society University Research Fellow. L.F. thanks the EU for a Marie Curie Fellowship (658271). S.C. thanks Imperial College London for a Schrödinger Scholarship. M.S thanks the Imperial College President's Ph.D. scholarship scheme. C.A.M acknowledges COLCIENCIAS for funding. S.G. acknowledges financial support from Ministerio de Ciencia, Innovación y Universidades of Spain (project ENE2017-85087-C3-1-R). This project has also received funding from the European Research Council (ERC) under the European Union's Horizon 2020 research and innovation programme (Grant Agreement No. 639750).

Competing interests

The authors declare no competing interests.

References

(1) Gan, J.; Lu, X.; Wu, J.; Xie, S.; Zhai, T.; Yu, M.; Zhang, Z.; Mao, Y.; Wang, S. C. I.; Shen, Y.; et al. Oxygen Vacancies Promoting Photoelectrochemical Performance of In2O3 Nanocubes. *Sci. Rep.* **2013**, *3* (1), 1021. https://doi.org/10.1038/srep01021.

(2) Wang, Z.; Mao, X.; Chen, P.; Xiao, M.; Monny, S. A.; Wang, S.; Konarova, M.; Du, A.; Wang, L. Understanding the Roles of Oxygen Vacancies in Hematite-Based Photoelectrochemical Processes. *Angew. Chemie - Int. Ed.* **2019**, *58* (4), 1030–1034. https://doi.org/10.1002/anie.201810583.

(3) Wu, J. M.; Chen, Y.; Pan, L.; Wang, P.; Cui, Y.; Kong, D. C.; Wang, L.; Zhang, X.; Zou, J. J. Multi-Layer Monoclinic BiVO4with Oxygen Vacancies and V4+species for Highly Efficient Visible-Light Photoelectrochemical Applications. *Appl. Catal. B Environ.* **2018**,

221 (August 2017), 187–195. https://doi.org/10.1016/j.apcatb.2017.09.031.

(4) Zhang, Y.; Guo, Y.; Duan, H.; Li, H.; Sun, C.; Liu, H. Facile Synthesis of V^{4+} Self-Doped, [010] Oriented $BiVO_4$ Nanorods with Highly Efficient Visible Light-Induced Photocatalytic Activity. *Phys. Chem. Chem. Phys.* **2014**, *16* (44), 24519–24526. https://doi.org/10.1039/C4CP03795B.

(5) Qin, D. D.; Wang, T.; Song, Y. M.; Tao, C. L. Reduced Monoclinic BiVO4 for Improved Photoelectrochemical Oxidation of Water under Visible Light. *Dalt. Trans.* **2014**, *43* (21), 7691–7694. https://doi.org/10.1039/c3dt53575d.

(6) Wang, S.; Chen, P.; Yun, J. H.; Hu, Y.; Wang, L. An Electrochemically Treated BiVO4 Photoanode for Efficient Photoelectrochemical Water Splitting. *Angew. Chemie - Int. Ed.* **2017**, *56* (29), 8500–8504. https://doi.org/10.1002/anie.201703491.

(7) Park, H. S.; Kweon, K. E.; Ye, H.; Paek, E.; Hwang, G. S.; Bard, A. J. Factors in the Metal Doping of BiVO4 for Improved Photoelectrocatalytic Activity as Studied by Scanning Electrochemical Microscopy and First-Principles Density-Functional Calculation. *J. Phys. Chem. C* **2011**, *115* (36), 17870–17879. https://doi.org/10.1021/jp204492r.

(8) Kim, T. W.; Ping, Y.; Galli, G. A.; Choi, K. S. Simultaneous Enhancements in Photon Absorption and Charge Transport of Bismuth Vanadate Photoanodes for Solar Water Splitting. *Nat. Commun.* **2015**, *6*, 1–10. https://doi.org/10.1038/ncomms9769.

(9) Wang, G.; Ling, Y.; Lu, X.; Qian, F.; Tong, Y.; Zhang, J. Z.; Lordi, V.; Rocha Leao, C.; Li, Y. Computational and Photoelectrochemical Study of Hydrogenated Bismuth Vanadate. *J. Phys. Chem. C* **2013**, *117* (21), 10957–10964. https://doi.org/10.1021/jp401972h.

(10) Yang, T. Y.; Kang, H. Y.; Sim, U.; Lee, Y. J.; Lee, J. H.; Koo, B.; Nam, K. T.; Joo, Y. C. A New Hematite Photoanode Doping Strategy for Solar Water Splitting: Oxygen Vacancy Generation. *Phys. Chem. Chem. Phys.* **2013**, *15* (6), 2117–2124. https://doi.org/10.1039/c2cp44352j.

(11) Corby, S.; Francàs, L.; Selim, S.; Sachs, M.; Blackman, C.; Kafizas, A.; Durrant, J. R. Water Oxidation and Electron Extraction Kinetics in Nanostructured Tungsten Trioxide Photoanodes. *J. Am. Chem. Soc.* **2018**, *140* (47), 16168–16177. https://doi.org/10.1021/jacs.8b08852.

(12) Sachs, M.; Park, J.; Pastor, E.; Kafizas, A.; Wilson, A. A.; Francàs, L.; Gul, S.; Ling, M.; Blackman, C.; Yano, J.; et al. Effect of Oxygen Deficiency on the Excited State Kinetics of WO3 and Implications for Photocatalysis. *Chem. Sci.* **2019**, *10* (22), 5667–5677. https://doi.org/10.1039/C9SC00693A.

(13) Crespillo, M. L.; Graham, J. T.; Agulló-López, F.; Zhang, Y.; Weber, W. J. Role of Oxygen Vacancies on Light Emission Mechanisms in SrTiO 3 Induced by High-Energy Particles. *J. Phys. D. Appl. Phys.* **2017**, *50* (15), 155303. https://doi.org/10.1088/1361-6463/aa627f.

(14) Crespillo, M. L.; Graham, J. T.; Agulló-López, F.; Zhang, Y.; Weber, W. J. Correlation between Cr 3+ Luminescence and Oxygen Vacancy Disorder in Strontium Titanate under MeV Ion Irradiation. *J. Phys. Chem. C* **2017**, *121* (36), 19758–19766. https://doi.org/10.1021/acs.jpcc.7b04352.

(15) Crespillo, M. L.; Graham, J. T.; Agulló-López, F.; Zhang, Y.; Weber, W. J. Isolated Oxygen Vacancies in Strontium Titanate Shine Red: Optical Identification of Ti3+ Polarons. *Appl. Mater. Today* **2018**, *12*, 131–137. https://doi.org/10.1016/j.apmt.2018.04.006.

(16) Chen, X.; Liu, L.; Huang, F. Black Titanium Dioxide (TiO2) Nanomaterials. *Chem. Soc. Rev.* **2015**, *44* (7), 1861–1885. https://doi.org/10.1039/C4CS00330F.

(17) Krol, R. Van De. *Photoelectrochemical Hydrogen Production*; 2012; Vol. 102. https://doi.org/10.1007/978-1-4614-1380-6.

(18) Le Formal, F.; Pendlebury, S. R.; Cornuz, M.; Tilley, S. D.; Gr??tzel, M.; Durrant, J. R. Back Electron-Hole Recombination in Hematite Photoanodes for Water Splitting. *J. Am. Chem. Soc.* **2014**, *136* (6), 2564–2574. https://doi.org/10.1021/ja412058x.

(19) Ma, Y.; Pendlebury, S. R.; Reynal, A.; Le Formal, F.; Durrant, J. R. Dynamics of Photogenerated Holes in Undoped BiVO4 Photoanodes for Solar Water Oxidation. *Chem. Sci.* **2014**, *5* (8), 2964–2973. https://doi.org/10.1039/c4sc00469h.

(20) Kafizas, A.; Ma, Y.; Pastor, E.; Pendlebury, S. R.; Mesa, C.; Francàs, L.; Le Formal, F.; Noor, N.; Ling, M.; Sotelo-Vazquez, C.; et al. Water Oxidation Kinetics of Accumulated Holes on the Surface of a TiO_2 Photoanode: A Rate Law Analysis. *ACS Catal.* **2017**, *7* (7), 4896–4903. https://doi.org/10.1021/acscatal.7b01150.

(21) Yuan, Y.; Huang, Y.; Ma, F.; Zhang, Z.; Wei, X. Effects of Oxygen Vacancy on the Mechanical, Electronic and Optical Properties of Monoclinic BiVO4. *J. Mater. Sci.* **2017**, *52* (14), 8546–8555. https://doi.org/10.1007/s10853-017-1069-7.

(22) Zhao, X.; Hu, J.; Yao, X.; Chen, S.; Chen, Z. Clarifying the Roles of Oxygen Vacancy in W-Doped $BiVO_4$ for Solar Water Splitting. *ACS Appl. Energy Mater.* **2018**, *1* (7), 3410–3419. https://doi.org/10.1021/acsaem.8b00559.

(23) Hu, J.; Zhao, X.; Chen, W.; Su, H.; Chen, Z. Theoretical Insight into the Mechanism of Photoelectrochemical Oxygen Evolution Reaction on $BiVO_4$ Anode with Oxygen Vacancy. *J. Phys. Chem. C* **2017**, *121* (34), 18702–18709. https://doi.org/10.1021/acs.jpcc.7b05884.

(24) Xiao, S.; Hu, C.; Lin, H.; Meng, X.; Bai, Y.; Zhang, T.; Yang, Y.; Qu, Y.; Yan, K.; Xu, J.; et al. Integration of Inverse Nanocone Array Based Bismuth Vanadate Photoanodes and Bandgap-Tunable Perovskite Solar Cells for Efficient Self-Powered Solar Water Splitting. *J. Mater. Chem. A* **2017**, *5* (36), 19091–19097. https://doi.org/10.1039/c7ta06309a.

(25) Walsh, A.; Yan, Y.; Huda, M. N.; Al-Jassim, M. M.; Wei, S.-H. H. Band Edge Electronic Structure of BiVO4 : Elucidating the Role of the Bi s and V d Orbitals. *Chem. Mater.* **2009**, *21* (3), 547–551. https://doi.org/10.1021/cm802894z.

(26) Cooper, J. K.; Gul, S.; Toma, F. M.; Chen, L.; Glans, P.; Guo, J.; Ager, J. W.; Yano, J.; Sharp, I. D. Electronic Structure of Monoclinic BiVO 4. **2014**.

(27) Ravensbergen, J.; Abdi, F. F.; van Santen, J. H.; Frese, R. N.; Dam, B.; van de Krol, R.; Kennis, J. T. M. Unraveling the Carrier Dynamics of BiVO 4 : A Femtosecond to Microsecond Transient Absorption Study. *J. Phys. Chem. C* **2014**, *118* (48), 27793–

27800. https://doi.org/10.1021/jp509930s.

(28) Cooper, J. K.; Reyes-Lillo, S. E.; Hess, L. H.; Jiang, C.-M.; Neaton, J. B.; Sharp, I. D. Physical Origins of the Transient Absorption Spectra and Dynamics in Thin-Film Semiconductors: The Case of BiVO 4. *J. Phys. Chem. C* **2018**, *122* (36), 20642–20652. https://doi.org/10.1021/acs.jpcc.8b06645.

(29) Grigioni, I.; Stamplecoskie, K. G.; Selli, E.; Kamat, P. V. Dynamics of Photogenerated Charge Carriers in WO 3 /BiVO 4 Heterojunction Photoanodes. *J. Phys. Chem. C* **2015**, *119* (36), 20792–20800. https://doi.org/10.1021/acs.jpcc.5b05128.

(30) Barroso, M.; Pendlebury, S. R.; Cowan, A. J.; Durrant, J. R. Charge Carrier Trapping, Recombination and Transfer in Hematite (α-Fe2O3) Water Splitting Photoanodes. *Chem. Sci.* **2013**, *4* (7), 2724. https://doi.org/10.1039/c3sc50496d.

(31) Pendlebury, S. R.; Wang, X.; Le Formal, F.; Cornuz, M.; Kafizas, A.; Tilley, S. D.; Grätzel, M.; Durrant, J. R. Ultrafast Charge Carrier Recombination and Trapping in Hematite Photoanodes under Applied Bias. *J. Am. Chem. Soc.* **2014**, *136* (28), 9854–9857. https://doi.org/10.1021/ja504473e.

(32) Huang, Z.; Lin, Y.; Xiang, X.; Rodríguez-Córdoba, W.; McDonald, K. J.; Hagen, K. S.; Choi, K.-S.; Brunschwig, B. S.; Musaev, D. G.; Hill, C. L.; et al. In Situ Probe of Photocarrier Dynamics in Water-Splitting Hematite (α-Fe2O3) Electrodes. *Energy Environ. Sci.* **2012**, *5* (10), 8923. https://doi.org/10.1039/c2ee22681b.

(33) Zandi, O.; Hamann, T. W. The Potential versus Current State of Water Splitting with Hematite. *Phys. Chem. Chem. Phys.* **2015**, *17* (35), 22485–22503. https://doi.org/10.1039/c5cp04267d.

(34) Klahr, B.; Hamann, T. Water Oxidation on Hematite Photoelectrodes: Insight into the Nature of Surface States through in Situ Spectroelectrochemistry. *J. Phys. Chem. C* **2014**, *118* (19), 10393–10399. https://doi.org/10.1021/jp500543z.

(35) Young, K. M. H.; Klahr, B. M.; Zandi, O.; Hamann, T. W. Photocatalytic Water Oxidation with Hematite Electrodes. *Catal. Sci. Technol.* **2013**, *3* (7), 1660–1671. https://doi.org/10.1039/c3cy00310h.

(36) Hayes, D.; Hadt, R. G.; Emery, J. D.; Cordones, A. A.; Martinson, A. B. F.; Shelby, M. L.; Fransted, K. A.; Dahlberg, P. D.; Hong, J.; Zhang, X.; et al. Electronic and Nuclear Contributions to Time-Resolved Optical and X-Ray Absorption Spectra of Hematite and Insights into Photoelectrochemical Performance. *Energy Environ. Sci.* **2016**, *9* (12), 3754–3769. https://doi.org/10.1039/C6EE02266A.

(37) Selim, S.; Francàs, L.; García-Tecedor, M.; Corby, S.; Blackman, C.; Gimenez, S.; Durrant, J. R.; Kafizas, A. WO 3 /BiVO 4 : Impact of Charge Separation at the Timescale of Water Oxidation. *Chem. Sci.* **2019**, *10* (9), 2643–2652. https://doi.org/10.1039/C8SC04679D.

(38) Yin, W.-J.; Wei, S.-H.; Al-Jassim, M. M.; Turner, J.; Yan, Y. Doping Properties of Monoclinic BiVO4 Studied by First-Principles Density-Functional Theory. *Phys. Rev. B* **2011**, *83* (15), 155102. https://doi.org/10.1103/PhysRevB.83.155102.

(39) Trześniewski, B. J.; Digdaya, I. A.; Nagaki, T.; Ravishankar, S.; Herraiz-Cardona, I.;

Vermaas, D. A.; Longo, A.; Gimenez, S.; Smith, W. A. Near-Complete Suppression of Surface Losses and Total Internal Quantum Efficiency in BiVO4photoanodes. *Energy Environ. Sci.* **2017**, *10* (6), 1517–1529. https://doi.org/10.1039/c6ee03677e.

(40) Rettie, A. J. E. E.; Lee, H. C.; Marshall, L. G.; Lin, J.-F.; Capan, C.; Lindemuth, J.; McCloy, J. S.; Zhou, J.; Bard, A. J.; Mullins, C. B. Combined Charge Carrier Transport and Photoelectrochemical Characterization of BiVO 4 Single Crystals: Intrinsic Behavior of a Complex Metal Oxide. *J. Am. Chem. Soc.* **2013**, *135* (30), 11389–11396. https://doi.org/10.1021/ja405550k.

(41) Rettie, A. J. E.; Chemelewski, W. D.; Lindemuth, J.; McCloy, J. S.; Marshall, L. G.; Zhou, J.; Emin, D.; Mullins, C. B. Anisotropic Small-Polaron Hopping in W:BiVO4 Single Crystals. *Appl. Phys. Lett.* **2015**, *106* (2), 0–5. https://doi.org/10.1063/1.4905786.

(42) Rettie, A. J. E.; Chemelewski, W. D.; Emin, D.; Mullins, C. B. Unravelling Small-Polaron Transport in Metal Oxide Photoelectrodes. *J. Phys. Chem. Lett.* **2016**, *7* (3), 471–479. https://doi.org/10.1021/acs.jpclett.5b02143.

(43) Bakulin, A. A.; Rao, A.; Pavelyev, V. G.; van Loosdrecht, P. H. M.; Pshenichnikov, M. S.; Niedzialek, D.; Cornil, J.; Beljonne, D.; Friend, R. H. The Role of Driving Energy and Delocalized States for Charge Separation in Organic Semiconductors. *Science (80-.).* **2012**, *335* (6074), 1340–1344. https://doi.org/10.1126/science.1217745.

(44) Hopper, T. R.; Gorodetsky, A.; Frost, J. M.; Müller, C.; Lovrincic, R.; Bakulin, A. A. Ultrafast Intraband Spectroscopy of Hot-Carrier Cooling in Lead-Halide Perovskites. *ACS Energy Lett.* **2018**, *3* (9), 2199–2205. https://doi.org/10.1021/acsenergylett.8b01227.

(45) Guyot-Sionnest, P.; Shim, M.; Matranga, C.; Hines, M. Intraband Relaxation in CdSe Quantum Dots. *Phys. Rev. B* **1999**, *60* (4), R2181–R2184. https://doi.org/10.1103/PhysRevB.60.R2181.

(46) Barroso, M.; Mesa, C. a; Pendlebury, S. R.; Cowan, A. J.; Hisatomi, T.; Sivula, K. Dynamics of Photogenerated Holes in Surface Modified α - Fe 2 O 3 Photoanodes for Solar Water Splitting. *Pnas* **2012**, *109*, 15640. https://doi.org/10.1073/pnas.1118326109/-/DCSupplemental.www.pnas.org/cgi/doi/10.1073/pnas.1118326109.

(47) Favaro, M.; Uecker, R.; Nappini, S.; Píš, I.; Magnano, E.; Bluhm, H.; van de Krol, R.; Starr, D. E. Chemical, Structural, and Electronic Characterization of the (010) Surface of Single Crystalline Bismuth Vanadate. *J. Phys. Chem. C* **2019**, *123* (13), 8347–8359. https://doi.org/10.1021/acs.jpcc.8b09016.

(48) Corby, S.; Pastor, E.; Dong, Y.; Zheng, X.; Francàs, L.; Sachs, M.; Selim, S.; Kafizas, A.; Bakulin, A. A.; Durrant, J. R. Charge Separation, Band-Bending, and Recombination in WO 3 Photoanodes. *J. Phys. Chem. Lett.* **2019**, *10* (18), 5395–5401. https://doi.org/10.1021/acs.jpclett.9b01935.

(49) Pastor, E.; Park, J.; Steier, L.; Kim, S.; Grätzel, M.; Durrant, J. R.; Walsh, A.; Bakulin, A. A. In Situ Observation of Picosecond Polaron Self-Localisation in α-Fe2O3 Photoelectrochemical Cells. *Nat. Commun.* **2019**, *10* (1), 3962. https://doi.org/10.1038/s41467-019-11767-9.

(50) Eichhorn, J.; Kastl, C.; Cooper, J. K.; Ziegler, D.; Schwartzberg, A. M.; Sharp, I. D.; Toma, F. M. Nanoscale Imaging of Charge Carrier Transport in Water Splitting Photoanodes. *Nat. Commun.* **2018**, *9* (1), 4–11. https://doi.org/10.1038/s41467-018-04856-8.

(51) Abdi, F. F.; Savenije, T. J.; May, M. M.; Dam, B.; Van De Krol, R. The Origin of Slow Carrier Transport in BiVO4 Thin Film Photoanodes: A Time-Resolved Microwave Conductivity Study. *J. Phys. Chem. Lett.* **2013**, *4* (16), 2752–2757. https://doi.org/10.1021/jz4013257.

(52) Zhang, L.; Ye, X.; Boloor, M.; Poletayev, A.; Melosh, N. A.; Chueh, W. C. Significantly Enhanced Photocurrent for Water Oxidation in Monolithic Mo:$BiVO_4$/SnO_2/Si by Thermally Increasing the Minority Carrier Diffusion Length. *Energy Environ. Sci.* **2016**, *9* (6), 2044–2052. https://doi.org/10.1039/C6EE00036C.

For Table of Contents Only